

# Biomechanical Role of Peri-Implant Cancellous Bone Architecture

Satoru Matsunaga, DDS, PhD<sup>a</sup>/Yoshitaka Shirakura, DDS<sup>b</sup>/Takashi Ohashi, DDS<sup>b</sup>/Ken Nakahara, DDS<sup>b</sup>/Yuichi Tamatsu, DDS, PhD<sup>c</sup>/Naoki Takano, PhD<sup>d</sup>/Yoshinobu Ide, DDS, PhD<sup>e</sup>

**Purpose:** The aim of this study was to investigate the biomechanical role of trabecular bone around dental implants in the mandible. **Materials and Methods:** The model in this study was made using micro-computed tomography data taken from a cadaver in whom endosseous implants had been in place for 15 years prior to death. Morphologic analysis and three-dimensional (3D) finite element analysis were performed to calculate the peri-implant loading path of the model in which the trabecular structure was accurately simulated. **Results:** As seen through multiscale analysis using the homogenization method, the trabecular bone architecture around implants was isotropic for the most part. Also, 3D finite element analysis showed that compressive stresses oblique to the implant axis were transmitted to the lower constrained surface; tensile stresses oblique to the implant axis were transmitted to the upper constrained surface, and they intersected each other with vertical loading. The highest stress in cancellous bone was observed on perpendicular loading, and stress produced in trabeculae decreased approaching horizontal loading. **Conclusion:** Cancellous bone architecture around the implant was generally isotropic. 3D finite element analysis showed that cancellous bone trabeculae around implants dispersed stress by forming load transfer paths. The results suggest that trabecular bone plays a major role in supporting functional pressure exerted via the implant. *Int J Prosthodont* 2010;23:333–338.

Dental implants are inserted into jaw bone. As a result, loads are transmitted directly to the peri-implant bone. Albrektsson et al reported that the loading condition was very important in the establishment and long-term maintenance of osseointegration.<sup>1</sup> If the functional loads via the implant exceed a certain force, they are regarded as being “overloaded.” Overloading

is considered one of the most serious pathologic factors and causes complications such as peri-implant bone resorption, screw loosening, and implant fracture.<sup>2,3</sup> Hence, it is essential to predict the supporting ability of the surrounding bone in implant surgery. However, there are few studies on the characteristics of jaw bone.

Factors affecting the success rate of osseointegrated implants include the load carrying capacity of cortical and cancellous bone. Recent studies have reported that the highest bone stresses occur in the cortical bone around the implant neck, depending on the load direction and type of stress/strain.<sup>4–6</sup> Previous studies did not take into account the anisotropy of cancellous bone in a numerical analysis of load dispersion around the implant. Even when using high-resolution medical computed tomography (CT), the resolving power is around 0.3 mm/voxel, which is not enough to delineate trabecular structures. Most three-dimensional (3D) finite element analyses simplify the cancellous bone to a block, completely ignoring its trabecular structure.<sup>4–7</sup> It is difficult to predict failure of a biomechanical etiology from the aforementioned analyses using a simplified

<sup>a</sup>Assistant Professor, Department of Anatomy, Tokyo Dental College, Chiba, Japan.

<sup>b</sup>Graduate Student, Department of Anatomy, Tokyo Dental College, Chiba, Japan.

<sup>c</sup>Associate Professor, Department of Neurology, Gross Anatomy Section, Kagoshima University Graduate School of Medical and Dental Sciences, Kagoshima University Dental School, Kagoshima, Japan.

<sup>d</sup>Professor, Department of Mechanical Engineering, Faculty of Science and Technology, Keio University, Kanagawa, Japan.

<sup>e</sup>Professor, Department of Anatomy, Tokyo Dental College, Chiba, Japan.

**Correspondence to:** Dr Satoru Matsunaga, Department of Anatomy, Tokyo Dental College, 1-2-2 Masago, Mihama-ku, Chiba-shi, Chiba-ken, 261-8502, Japan. Fax: +81-43-277-4010. Email: matsuna@tdc.ac.jp

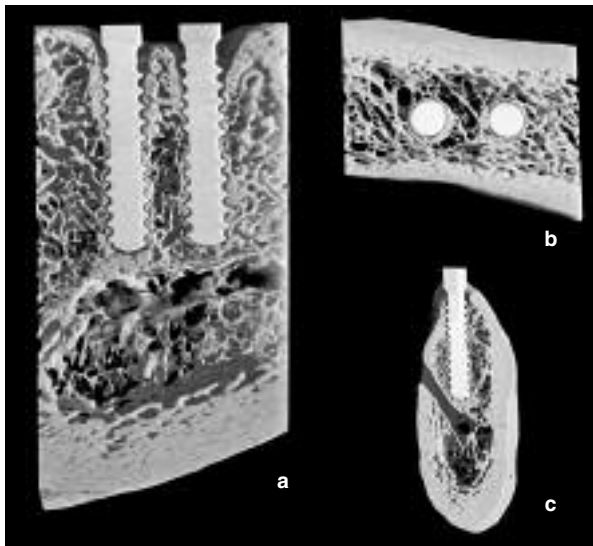


**Fig 1** Reconstructed 3D images cut along (a) the sagittal plane, (b) the horizontal plane, and (c) the frontal plane.

model. Stegaroiu et al<sup>8</sup> compared a precise model with a trabecular structure to a simplified model and reported that analysis error occurred in the cancellous bone area. Therefore, it is necessary to determine the load transfer paths around an implant using a precise model in which the trabecular structure is simulated accurately to clarify the supporting function of the peri-implant bone.

In addition, recent studies have suggested that the trabecular structure of cancellous bone is closely related to bone strength. Therefore, the macroscopic properties of trabecular bone have gained considerable attention in mechanobiology.<sup>9-11</sup> Hollister et al<sup>12</sup> and Lin et al<sup>13</sup> employed the homogenization technique used in mechanical engineering to calculate the macroscopic characteristics of cancellous bone. It is necessary to evaluate macroscopic properties to understand the characteristics of porous materials such as cancellous bone. Furthermore, microscopic stress distribution in addition to homogenized macroscopic properties can be clarified by multiscale analysis using the homogenization method.<sup>14</sup> Using this method, it is possible to ascertain the trabecular anisotropy by analyzing macrorigidity, which reflects the trabecular structures.

In the present study, the anisotropy of peri-implant bone trabeculae was quantified by multiscale analysis using the homogenization method, and load transfer paths were visualized to clarify the role of peri-implant cancellous bone.

## Materials and Methods

The mandible was removed from the cadaver of an 82-year-old man donated for dissection in whom endosseous implants had been in place for 15 years prior to death. Screw-type 4.1-mm implants were placed in the right first and second premolar sites. These regions were detached from the mandible and used as the specimen.

### Micro-CT Imaging

The mandible was scanned using a micro-CT system (HMX-225 Actis4, Tesco). Imaging was performed under the following conditions: tube voltage = 120 kV, tube current = 200  $\mu$ A, and slice width = 50  $\mu$ m. A 4-inch image intensifier was used that had a 1-inch charge-coupled device camera with 16-bit  $1,024 \times 1,024$  scanning lines. The camera generated 1,200 raw data images. Based on the raw data, 2D sliced data were prepared by the back projection method. The mandible was scanned at the right first and second premolar regions from the upper part of implant (excluding the abutment) to the lower margin of the mandible (Fig 1).

### Multiscale Analysis Using the Homogenization Method

Multiscale analysis was accomplished to evaluate anisotropy of the trabecular bone structure surrounding the implants (DoctorBQ, KGT and Quint). The homogenization method is a mathematic theory that calculates the macroscopic properties of structures with microscopic heterogeneity, such as composite materials or porous ceramics. A microscopic region containing all characteristics, enough to represent the global trabecular bone heterogeneity, was extracted to describe the bone density distribution. Eight micro-analysis areas were extracted on the basis of bone volume fraction (Figs 2 and 3). Periodicity for displacements was applied as the boundary condition for these microanalyses. To this end, macroscopic Young modulus and Poisson ratio were calculated.

### Load Transfer Paths

**Finite Element Model.** Analysis areas were set within the CT imaging range. After removing unnecessary features, each preprocessed 3D image for finite element analysis was downsized and subjected to binarization based on a threshold value obtained by the discriminate analysis thresholding method. After labeling, mapping was performed using eight-node hexahedral elements ( $1 \text{ voxel} = 0.076 \times 0.076 \times 0.076 \text{ mm}^3$ ). The

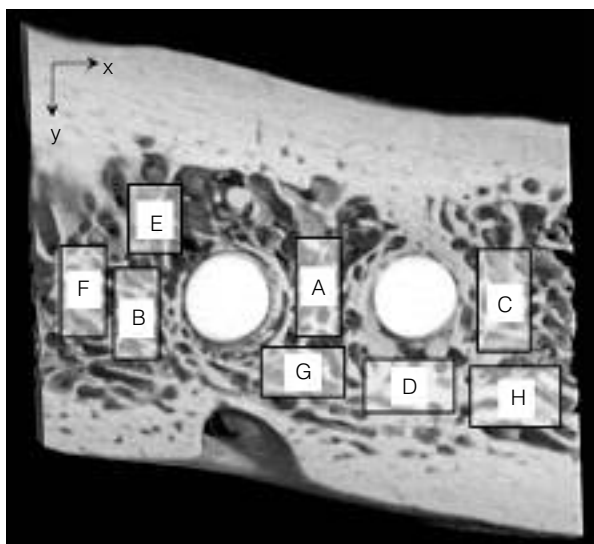


**Fig 2** Eight adaptive microanalysis areas were selected (A through H) and the homogenization method was applied to calculate the microscopic properties.

total number of nodes and elements were 6,870,990 and 5,993,510, respectively. For the boundary between the mandible and implants, contact areas were considered connected.

**Constitutive Laws.** Model components were the bone and implants, and both were considered linear isotropic materials. The Young modulus and Poisson ratio for bone were set at 15 GPa and 0.30, respectively, and those for implants were set at 110 GPa and 0.35, respectively.<sup>15,16</sup>

**Boundary Condition.** Analysis of the finite element model was performed using finite element software. All nodes at the mesiodistal plane of the mandibular body were constrained in all directions (Fig 4). A 250-nm strain was applied to the top of the implant at angles of 15, 45, and 90 degrees to the occlusal plane.

**Output.** Maximum principal stress distribution and vector were evaluated with an output program (DoctorBQ, KGT and Quint). At the same time, the deformation mode with a 5,000-fold increase in strain was observed dynamically.

## Results

### **Multiscale Analysis Using the Homogenization Method**

Table 1 shows the homogenized elastic and shear moduli in the microscopic region. Figure 5 shows the approximating curve of bone volume fraction and homogenized properties. The trabecular bone architecture around implants was isotropic for the most part.

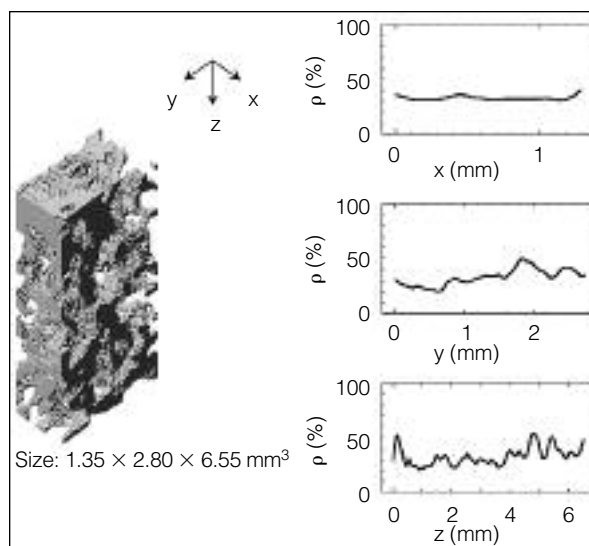


**Fig 3** Microanalysis areas were extracted on the basis of bone volume fraction.  $\rho$  = bone density.

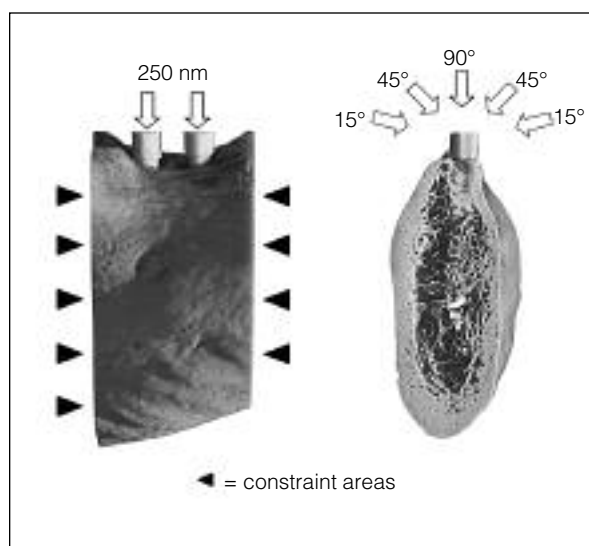


**Fig 4** Constraint areas and loads.

### **Load Transfer Paths**

Compressive stresses oblique to the implant axis were transmitted to the lower constrained surface; tensile stresses oblique to the implant axis were transmitted to the upper constrained surface and they intersected one another (Figs 6 and 7). In cortical bone, higher tensile stresses were generated at the neck of the implant.

**Table 1** Homogenized Elastic Constants and Shear Modulus

Homogenized material properties		
A (BV/TV = 32.8)		
$E_x, E_y, E_z$	1.21, 1.17, 1.34	
$G_{xy}, G_{yz}, G_{zx}$	0.39, 0.42, 0.45	
$V_{xy}, V_{yz}, V_{zx}$	0.21, 0.18, 0.20	
B (BV/TV = 39.4)		
$E_x, E_y, E_z$	1.86, 1.76, 2.06	
$G_{xy}, G_{yz}, G_{zx}$	0.64, 0.66, 0.76	
$V_{xy}, V_{yz}, V_{zx}$	0.20, 0.19, 0.23	
C (BV/TV = 58.0)		
$E_x, E_y, E_z$	4.27, 4.84, 4.13	
$G_{xy}, G_{yz}, G_{zx}$	1.78, 1.72, 1.47	
$V_{xy}, V_{yz}, V_{zx}$	0.22, 0.23, 0.20	
D (BV/TV = 83.4)		
$E_x, E_y, E_z$	10.20, 9.04, 10.45	
$G_{xy}, G_{yz}, G_{zx}$	3.66, 3.75, 3.97	
$V_{xy}, V_{yz}, V_{zx}$	0.27, 0.13, 0.27	
E (BV/TV = 17.8)		
$E_x, E_y, E_z$	0.29, 0.43, 0.27	
$G_{xy}, G_{yz}, G_{zx}$	0.10, 0.11, 0.08	
$V_{xy}, V_{yz}, V_{zx}$	0.11, 0.23, 0.16	
F (BV/TV = 35.2)		
$E_x, E_y, E_z$	0.78, 1.18, 0.96	
$G_{xy}, G_{yz}, G_{zx}$	0.37, 0.39, 0.34	
$V_{xy}, V_{yz}, V_{zx}$	0.16, 0.24, 0.23	
G (BV/TV = 44.8)		
$E_x, E_y, E_z$	2.14, 1.19, 1.91	
$G_{xy}, G_{yz}, G_{zx}$	0.55, 0.55, 0.77	
$V_{xy}, V_{yz}, V_{zx}$	0.26, 0.17, 0.20	
H (BV/TV = 63.9)		
$E_x, E_y, E_z$	4.05, 2.52, 4.14	
$G_{xy}, G_{yz}, G_{zx}$	1.16, 1.19, 1.63	
$V_{xy}, V_{yz}, V_{zx}$	0.29, 0.18, 0.24	

Input: Longitudinal elastic coefficient = 15 GPa.  
 Poisson ratio = 0.30.  
 BV/TV = Bone volume fraction (%); E = longitudinal elastic volume (GPa); G = transverse elastic coefficient (GPa); V = Poisson ratio.

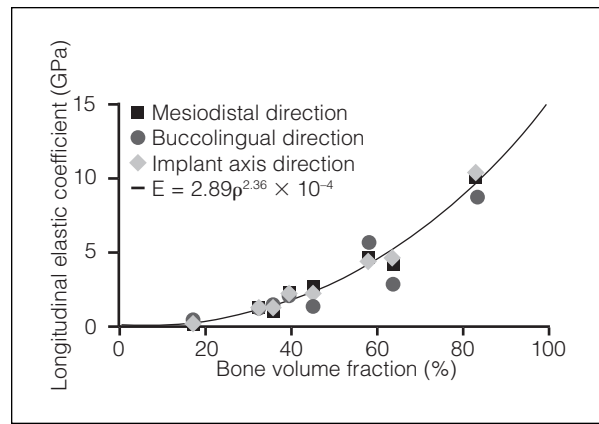


**Fig 5** Relationship between homogenized Young modulus and bone volume fraction indicating the mechanical properties showing the exponential function in each microanalysis area.

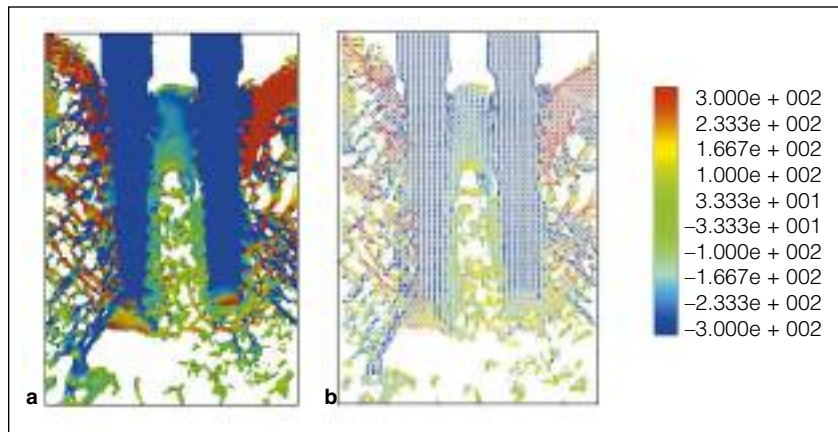


**Fig 6** Load transfer path at the mesiodistal section. (a) Contour plot, (b) vector plot.

On the other hand, comparatively lower stresses were generated at the trabecular bone connecting the implants. The deformation mode showed that the two implants reacted as one unit against loads, and the peri-implant trabecular bone architecture dispersed the loads by forming a hammock-like structure (Fig 8).

The highest stress in cancellous bone was observed on perpendicular loading, and stress produced in trabeculae decreased approaching horizontal loading (Figs 9a and 9b). On the other hand, stress concentration was seen in the cortical bone around the implants on application of a horizontal load, as seen with a vertical load.

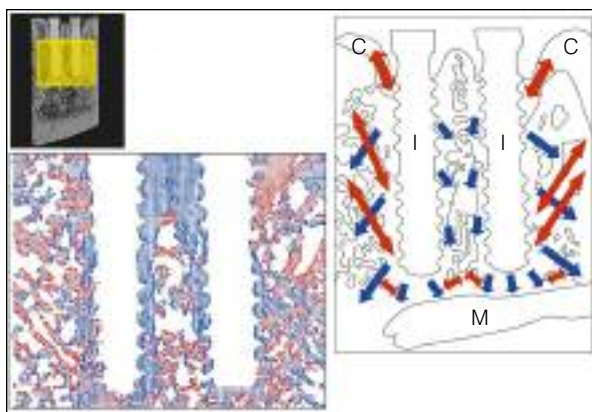


**Fig 7** The simplified image of Fig 6. Blue arrow = compression stress; red arrow = tensile stress; C = cortical bone; I = implant; M = mandibular canal.

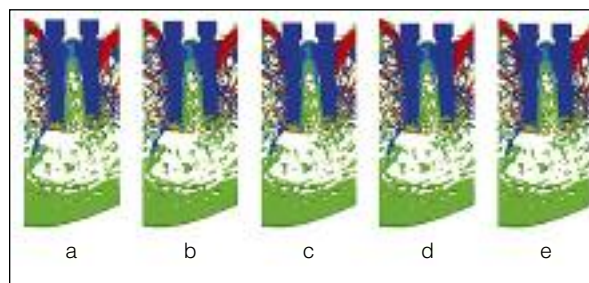


**Fig 8** Each stage of deformation occurring in the trabecular structure due to the applied load in order from a to e.

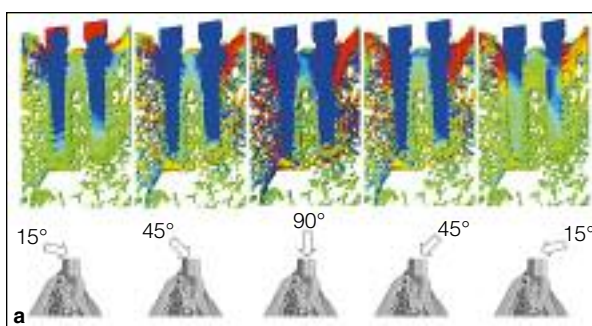
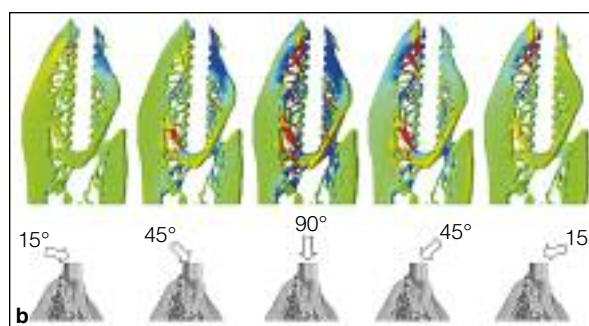


**Fig 9** Comparison with load angle in the (a) mesiodistal section and (b) buccolingual section.



## Discussion

Recent papers on bone biomechanics have discussed the need to consider trabecular bone architecture.<sup>17-19</sup> Verhulst and colleagues<sup>17</sup> reported that stresses were dispersed by trabecular bone at the proximal head of the femur. Homminga et al<sup>18</sup> suggested that a strong relationship existed between trabecular bone architecture and bone strength. In the Consensus Development Conference Statement published by the National Institute of Health in 2000,<sup>20</sup> evaluation of bone density, including factors such as cancellous bone architecture, turnover, damage accumulation, and mineralization, was recommended. In contrast, the jaw bones have a complicated morphology because of stresses being received from numerous directions; therefore, it is difficult to consider the cancellous bone architecture.

Dental implants are widely used as substitutes for missing teeth to regain masticatory function. However, because the dental implant bonds directly to the jaw

bone, it is well known that the biomechanical effect of the implant is greater than that of teeth.<sup>21-23</sup> It was necessary to quantify the anisotropy of peri-implant bone trabeculae and observe the load transfer paths to investigate the influence of mechanical stress transmitted via the implant to the trabecular bone structure.

Through multiscale analysis, a correlation between Young modulus and bone density was found, and the 3D bone architecture around the implant was generally isotropic. The authors speculated that this was caused by complicated functional pressure.

This study simulated bone as an isotropic material and observed load transfer paths. In previous stress analyses, von Mises equivalent stress and maximum principal stress could only be expressed in numerical values and colors as a contour plot, and it was possible to assess the extent but not the direction of the stress. The maximum principal stress vector for all elements was expressed stereoscopically to confirm the load transfer paths.

Previous studies showed that peri-implant cortical bone dispersed stress. Cancellous bone trabeculae around implants dispersed stress by forming load transfer paths. The results obtained in this study suggest that not only cortical bone but also cancellous bone play a major role in supporting the functional pressure exerted via the implant.

In the present study, because there was access to a mandible in which endosseous implants had been in place for a long period of time, the mandible was analyzed by micro-CT, and then a model of the mandible and its surrounding microstructures was prepared. Therefore, the authors assumed that simulated load transfer paths in this study reflected a living body. However, the specimen used was only one cadaver so the result could not be concluded accurately.

## Conclusions

Cancellous bone architecture around the implant was generally isotropic. Three-dimensional finite element analysis showed that cancellous bone trabeculae around implants dispersed stress by forming load transfer paths. The results suggest that trabecular bone plays a major role in supporting functional pressure exerted via the implant.

## Acknowledgments

This study was supported by an Oral Health Science Center Grant (no. 5A10) from Tokyo Dental College and by a Grant-in-Aid for Scientific Research (nos. 19592259 and 20791441) from the Ministry of Education, Culture, Sports, Science, and Technology, Japan. The authors would like to thank Prof M. Hashimoto of the Department of Forensic Anthropology of Tokyo Dental College for his thoughtful review of the manuscript. The authors also appreciate the enthusiastic cooperation of the staff of the Department of Anatomy, Tokyo Dental College.

## References

- Albrektsson T, Brånemark PI, Hansson HA, Lindström J. Osseointegrated titanium implants. Requirements for ensuring a long-lasting, direct bone-to-implant anchorage in man. *Acta Orthop Scand* 1981;52:155-170.
- Esposito M, Hirsch JM, Lekholm U, Thomsen P. Biological factors contributing to failures of osseointegrated oral implants. (II). Etiopathogenesis. *Eur J Oral Sci* 1998;106:721-764.
- Esposito M, Hirsch J, Lekholm U, Thomsen P. Differential diagnosis and treatment strategies for biologic complications and failing oral implants: A review of the literature. *Int J Oral Maxillofac Implants* 1999;14:473-490.
- O'Mahony AM, Williams JL, Spencer P. Anisotropic elasticity of cortical and cancellous bone in the posterior mandible increases peri-implant stress and strain under oblique loading. *Clin Oral Implants Res* 2001;12:648-657.
- Sütçüder M, Eckert SE, Zobitz M, An KN. Finite element analysis of effect of prosthesis height, angle of force application, and implant offset on supporting bone. *Int J Oral Maxillofac Implants* 2004;19:819-825.

- Eskitascioglu G, Usumez A, Sevımay M, Soykan E, Unsal E. The influence of occlusal loading location on stresses transferred to implant-supported prostheses and supporting bone: A three-dimensional finite element study. *J Prosthet Dent* 2004;91:144-150.
- Stegarioiu R, Sato T, Kusakari H, Miyakawa O. Influence of restoration type on stress distribution in bone around implants: A three-dimensional finite element analysis. *Int J Oral Maxillofac Implants* 1998;13:82-90.
- Stegarioiu R, Watanabe N, Tanaka M, Ejiri S, Nomura S, Miyakawa O. Peri-implant stress analysis in simulation models with or without trabecular bone structure. *Int J Prosthodont* 2006;19:40-42.
- Mosekilde L, Ebbesen EN, Tornvig L, Thomsen JS. Trabecular bone structure and strength—Remodeling and repair. *J Musculoskelet Neuronal Interact* 2000;1:25-30.
- Teo JC, Si-Hoe KM, Keh JE, Teoh SH. Relationship between CT intensity, micro-architecture and mechanical properties of porcine vertebral cancellous bone. *Clin Biomech* 2006;21:235-244.
- Yi WJ, Heo MS, Lee SS, Choi SC, Huh KH. Comparison of trabecular bone anisotropies based on fractal dimensions and mean intercept length determined by principal axes of inertia. *Med Biol Eng Comput* 2007;45:357-364.
- Hollister SJ, Brennan JM, Kikuchi N. A homogenization sampling procedure for calculating trabecular bone effective stiffness and tissue level stress. *J Biomech* 1994;27:433-444.
- Lin CY, Kikuchi N, Hollister SJ. A novel method for biomaterial scaffold internal architecture design to match bone elastic properties with desired porosity. *J Biomech* 2004;37:623-636.
- Takano N, Zako M, Kubo F, Kimura K. Microstructure-based stress analysis and evaluation for porous ceramics by homogenization method with digital image-based modeling. *Int J Solid Struct* 2003;40:1225-1242.
- Turner CH, Rho J, Takano Y, Tsui TY, Pharr GM. The elastic properties of trabecular and cortical bone tissues are similar: Results from two microscopic measurement techniques. *J Biomech* 1999;32:437-441.
- Geng JP, Tan KB, Liu GR. Application of finite element analysis in implant dentistry: A review of the literature. *J Prosthet Dent* 2001;85:585-598.
- Verhulst E, Van Rietbergen B, Muller R, Huiskes R. Micro-finite element simulation of trabecular-bone post-yield behaviour—Effects of material model, element size and type. *Comput Methods Biomech Biomed Engin* 2008;11:389-395.
- Homminga J, Van Rietbergen B, Lochmüller EM, Weinans H, Eckstein F, Huiskes R. The osteoporotic vertebral structure is well adapted to the loads of daily life, but not to infrequent "error" loads. *Bone* 2004;34:510-516.
- Boyd SK, Müller R. Smooth surface meshing for automated finite element model generation from 3D image data. *J Biomech* 2006;39:1287-1295.
- Osteoporosis prevention, diagnosis, and therapy. *NIH Consensus Statement* 2000;17:1-45.
- Williams WN, Levin AC, LaPointe LL, Cornell CE. Bite force discrimination by individuals with complete dentures. *J Prosthet Dent* 1985;54:146-150.
- Chapman RJ. Principles of occlusion for implant prostheses: Guidelines for position, timing, and force of occlusal contacts. *Quintessence Int* 1989;20:473-480.
- Richter EJ. Basic biomechanics of dental implants in prosthetic dentistry. *J Prosthet Dent* 1989;61:602-609.

Copyright of International Journal of Prosthodontics is the property of Quintessence Publishing Company Inc. and its content may not be copied or emailed to multiple sites or posted to a listserv without the copyright holder's express written permission. However, users may print, download, or email articles for individual use.